Int. J. Heat Mass Transfer. Vol. 35, No. 2, pp. 545–557, 1992
Printed in Great Britain

0017–9310/92 $5.00 + 0.00
© 1992 Pergamon Press plc

Laminar natural convection in a cylindrical enclosure with different end temperatures

STEFAN SCHNEIDER and JOHANNES STRAUB
Lehrstuhl A für Thermodynamik, Technische Universität München, P.O. Box 202420, D-8000 Munich 2, F.R.G.

(*Received* 14 *November* 1990)

Abstract—Laminar natural convection in a fluid-filled cylinder with different end wall temperatures is investigated in a three-dimensional numerical study and is experimentally verified. The influences of fluid and geometrical parameters, like Rayleigh number ($Ra < 8 \times 10^4$), Prandtl number ($0.023 \leqslant Pr \leqslant 135$), aspect ratio height/diameter ($0.5 \leqslant H/D \leqslant 2$), and inclination angle ($0° \leqslant \alpha \leqslant 180°$) on convective motion and heat transfer are presented. Maximum heat transfer and greatest velocities are found for $H/D = 1$ at inclination angles of $\alpha \approx 45°–60°$.

1. INTRODUCTION

DENSITY differences in a fluid, caused by concentration or temperature differences, lead to buoyancy forces in the presence of a gravitational field. The resulting fluid motion, known as natural convection, plays an important role in many technical applications dealing with a differentially heated fluid as in heating or cooling devices, solar collectors, crystal growth or solidification processes, etc. In this paper, only natural convection caused by temperature differences is studied.

Many theoretical and experimental contributions deal with natural convection in fluid layers of large horizontal extension heated from below. These publications study the critical Rayleigh number, at which convective motion starts, the establishing of flow modes and their changes with varying Rayleigh number. Heat transfer is generally less emphasized. A review on this topic is given by Koschmieder [1]. The case of a vertical fluid layer heated from the side is also studied frequently. This configuration is investigated for a great variety of aspect ratios, especially for rectangular enclosures. Only very few works deal with cylindrical enclosures heated at one end wall and cooled at the other one, when the cylinder axis is horizontal. Furthermore, these contributions are restricted to cylinders of height-to-diameter ratios of $H/D \geqslant 5$, and only treat the flow field, not the heat transfer [2–9].

The limited number of publications in this field is probably a consequence of the flow field being three-dimensional. Therefore, it cannot easily be treated theoretically or numerically. Experimentation with optical methods is also difficult due to cylindrical refraction effects.

Only a single study [10] is known to the authors treating the influence of the inclination of the cylinder axis with respect to the direction of gravity. It describes the flow structure in a cylinder with an aspect ratio of $H/D = 5$ with perfectly conducting lateral walls being inclined in the range of $\alpha = 20°–90°$ (Fig. 1). For rectangular cavities, there are some publications on the influence of the inclination angle [11–24]; but owing to the different geometry compared to a cylinder, the flow structure might be different, and the results are not comparable.

The main objective of this study is to clarify the dependence of the flow field and the heat transfer on the inclination angle, furthermore, to study the influences of the Rayleigh number, the Prandtl number and the aspect ratio H/D. A numerical code has been developed to calculate both transient and steady-state natural three-dimensional convection in a cylindrical enclosure [25–27]. The results of this theoretical study are compared with the findings from the literature and our own experiments, and satisfactory agreement is obtained.

2. PHYSICAL AND MATHEMATICAL MODELS

2.1. *Basic equations*

The geometry of the problem is shown in Fig. 1. Using the so-called Boussinesq approximation, the temperature dependence of the fluid density is taken into account only in the buoyancy term of the equation of motion. At all other appearances, a mean value ρ_m defined at an average temperature ($T_m = \frac{1}{2}(T_{hot} + T_{cold})$) is used. All the other properties are assumed to be constant. The time-dependent three-dimensional buoyancy-driven flow in a cylindrical enclosure (filled with gas or liquid) is governed by the following equations (compressive work and viscous dissipation are neglected):

equation of continuity

$$\nabla \cdot \mathbf{v}^* = 0; \tag{1}$$

NOMENCLATURE

c_p	specific heat
C	wall admittance according to Catton [39]
D	inner diameter
Fo	Fourier number, $\kappa t/D^2$
g	gravitational acceleration
H	height of the cylinder
H/D	aspect ratio
k	thermal conductivity
L	characteristic length
Nu	Nusselt number, $(\partial T/\partial z)\|_{z=0}/((T_{\text{cold}}-T_{\text{hot}})/H)$
p	pressure
Pr	Prandtl number, ν/κ
r	radial coordinate
R	inner radius of the cylinder
R_0	gas law constant
Ra	Rayleigh number, $g\beta_p L^3(T_{\text{hot}}-T_{\text{cold}})/\nu\kappa$
t	time
T	temperature
v	velocity
z	axial coordinate.

Greek symbols

α	inclination angle
β_p	thermal expansion coefficient, $(-1/\rho)\times(\partial\rho/\partial T)_p$
κ	thermal diffusivity
μ	dynamic viscosity
ν	kinematic viscosity
ρ	density
φ	azimuthal coordinate.

Subscripts

cold	cold wall
crit	critical value
D	diameter D as characteristic length scale
fluid	fluid
hot	hot wall
H	height H as characteristic length scale
max	maximum value
r	radial component
z	axial component
φ	azimuthal component
0	reference value
∞	ambient.

Superscript

*	dimensional variable (only noted if there is a dimensionless variable of the same name).

equation of motion

$$\rho\frac{\mathrm{D}\mathbf{v}^*}{\mathrm{D}t} = -\nabla p+\mu\nabla^2\mathbf{v}^*+\rho\mathbf{g}; \tag{2}$$

equation of energy

$$\rho c_p\frac{\mathrm{D}T}{\mathrm{D}t} = k\nabla^2 T. \tag{3}$$

With the differential operators

$$\frac{\mathrm{D}}{\mathrm{D}t} = \frac{\partial}{\partial t}+v_r^*\frac{\partial}{\partial r}+\frac{v_\varphi^*}{r}\frac{\partial}{\partial\varphi}+v_z^*\frac{\partial}{\partial z}$$

$$\nabla = \frac{1}{r}\frac{\partial}{\partial r}r+\frac{1}{r}\frac{\partial}{\partial\varphi}+\frac{\partial}{\partial z}$$

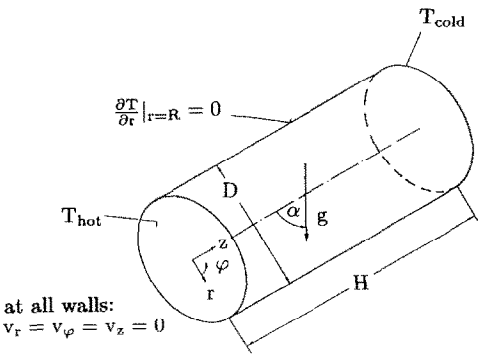

FIG. 1. Scheme of the cylinder and the boundary conditions.

$$\nabla^2 = \frac{1}{r}\frac{\partial}{\partial r}\left(r\frac{\partial}{\partial r}\right)+\frac{1}{r^2}\frac{\partial^2}{\partial\varphi^2}+\frac{\partial^2}{\partial z^2}.$$

For gases, the temperature dependence of the density is described by the equation of state for an ideal gas

$$\rho = \frac{p}{R_0 T} \tag{4a}$$

while for liquids the density is calculated from

$$\rho = \rho_0[1-\beta_p(T-T_0)]. \tag{4b}$$

We assume no-slip conditions at all walls.

The thermal boundary conditions are as follows:

isothermal top and bottom walls

$$T(r,\varphi,0) = T_{\text{hot}} \tag{5}$$

$$T(r,\varphi,H) = T_{\text{cold}}; \tag{6}$$

perfectly insulated lateral wall (adiabatic)

$$\left.\frac{\partial T}{\partial r}\right|_{r=R} = 0; \tag{7a}$$

or perfectly conducting lateral wall

$$T(R,\varphi,z) = T_{\text{cold}}+(T_{\text{hot}}-T_{\text{cold}})\left(1-\frac{z}{H}\right). \tag{7b}$$

Aspect ratio, inclination angle of the cylinder axis

with the direction of the gravity field, Prandtl and Rayleigh numbers can optionally be varied. The following dimensionless variables are used:

Rayleigh number

$$Ra = \frac{g\beta_p L^3 (T_{hot} - T_{cold})}{\nu\kappa};$$

Prandtl number

$$Pr = \frac{\nu}{\kappa};$$

Fourier number

$$Fo = t\frac{\kappa}{D^2};$$

dimensionless velocity

$$\mathbf{v} = \mathbf{v}^* \frac{D}{\kappa}.$$

As a rule for choosing the correct characteristic length for scaling, usually the dimension in the direction of gravity is used. This rule is applicable for $\alpha = 0°$ ($L = H$) and 90° ($L = D$). For other inclinations, we tried to consider the inclination effect by choosing a modified Rayleigh number expressed in terms of the cylinder's extension in the gravity direction. This approach, however, was not successful. As a result, we take the diameter D as the characteristic length L in the scaling equations mentioned above. When the inclination angle varies, while the Rayleigh number is kept constant, no other variable (e.g. temperature difference) has to be changed. By this approach, comparability of results obtained at different inclination angles is achieved.

2.2. *Method of solution*

The numerical code is based upon a finite volume method with explicit time steps and a semi-iterative pressure–velocity correction (SIMPLE algorithm [28]). By using an equidistant mesh ($\Delta r = \text{const.}$, $\Delta\varphi = \text{const.}$, $\Delta z = \text{const.}$) the partial differential equations are discretized. The algebraic equations are formulated in dimensional form in terms of 'primitive' variables (v_r^*, v_φ^*, v_z^*, p, T, ρ).

Temperature, density and pressure are defined in the centres of the finite volumes. The velocities are calculated for points lying in the middle of the faces of the control volumes ('staggered grid' [29]). Figure 2 shows the grid arrangement in radial and axial cross-sections. Using cylindrical coordinates the treatment of the cylinder axis is often a problem for numerical schemes, because some terms of the basic equations become indefinite for $r = 0$. deVahl Davis [30] suggested leaving the cylinder axis out of the consideration. Thus, not a real cylinder, but an annulus with a small inner diameter is calculated. This concept is widely used in the literature [3–5, 10]. We developed a different method for solving this problem that seems

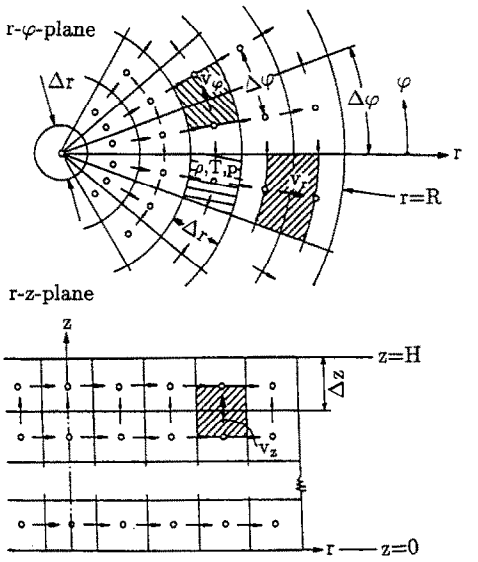

FIG. 2. Grid arrangement in the r–φ and r–z planes.

to be more appropriate for non-axisymmetric problems: we use a cylindrical volume element of diameter Δr for the axis. On the axis, v_z, p, T, and ρ are defined. Azimuthal velocities cannot exist at $r = 0$, and radial velocities are calculated at points on the radial face of the volume element ($r = \Delta r/2$). Thus, the whole cylinder can be calculated without further restrictions.

As we are interested in the transient, as well as in the steady-state fluid behaviour [25–27, 31], the stationary results are obtained as the final state of the transient calculations. The computing costs of transient three-dimensional calculations are generally high, especially when a fine mesh is used. Our primary interest was to concentrate on the study of various parameter dependencies rather than the absolute accuracy of the calculated results. Therefore, quite a coarse mesh is used as a reasonable compromise between accuracy and computing costs. If one compares two results achieved with the same mesh, while the same flow mode is observed, then the relationship of these computed results is assumed to be correct, even though the absolute values are less accurate. Furthermore, the calculated flow structure is shown to be correct [25]. There is no doubt, if a finer mesh had been applied, the accuracy would have been increased, but we would not have been able to vary the parameters up to the desired extent.

The number of grid points is chosen depending on the aspect ratio and the Rayleigh number. It is denoted by (A, B, C), where A describes the number of points in the radial, B the azimuthal, and C the axial directions. The central element and additional elements needed to formulate the boundary and coupling conditions are not included in these numbers.

3. NUMERICAL RESULTS

In a cylinder of aspect ratio of $H/D \geqslant 1$, a single flow roll with upflow at the warm and downflow at

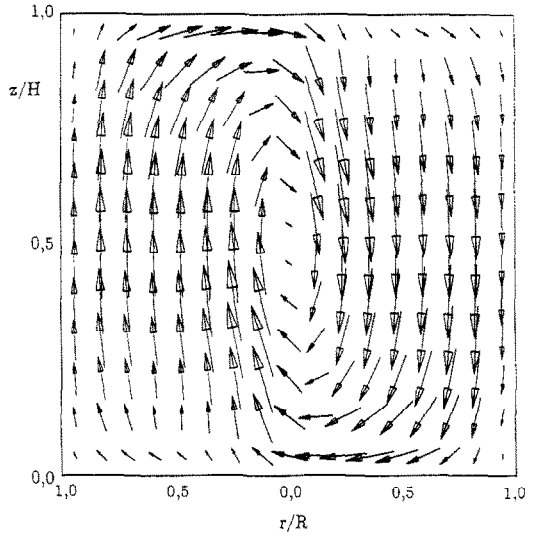

FIG. 3. Flow field in a vertical cross-section ($Ra = 5000$, $H/D = 1$, $\alpha = 90°$, liquid silicon).

the cold wall is observed in all cases studied (Fig. 3). For $H/D = 1/2$ and $1/4$, axisymmetric flow modes are found for the vertical cylinder $\alpha = 0°$, and single flow rolls when the cylinder is inclined to 2.5° (Fig. 4).

The transient and steady-state flow fields are calculated completely. Since the representation of the flow by plots of the whole velocity field is too voluminous, the intensity of fluid motion is only described by the maximum velocities. Even if location and direction of the maximum velocity may vary, its magnitude is an upper limit for all fluid velocities. The heat transfer is characterized by the Nusselt number averaged over the hot end wall, which is, for steady-state conditions, equal to the one at the cold end wall.

3.1. *Critical Rayleigh number*

In all cases where the inclination angle is different from $\alpha = 0°$, no unstable stratified fluid layer can be formed. In reality, convection starts instantaneously with heating, while the numerical calculation accounts for this effect at the first time step. If $\alpha = 0°$ (the heated end wall is at the bottom), an unstable fluid layer is formed, and a small disturbance of this layer leads to the onset of convection. This is well known as the Rayleigh–Bénard problem, which is solved with different methods for the horizontal infinitely extended system. The critical Rayleigh number for the onset of motion is found to be $Ra_{crit} = 1708$. Lateral walls stabilize the stratified fluid layer. So the critical Rayleigh number is shifted to higher values, as the fluid layer's horizontal extent shrinks.

As a test for our numerical code, critical Rayleigh numbers are determined for vertical gas-filled cylinders ($Pr = 0.71$) of various aspect ratios with perfectly insulated lateral walls. The initial conditions are as follows: no motion ($v_r^* = v_\varphi^* = v_z^* = 0$), a linear temperature profile in the axial direction ($\partial T/\partial z = (T_{cold} - T_{hot})/H$), and a hydrostatic pressure field ($\partial p/\partial z = -\rho(T_m)\, g$). To obtain Ra_{crit}, the fluid's transient reaction to a small perturbation during the first time step is studied, which is either a small inclination $\alpha = 0.2°$ ($H/D \geqslant 1$) or an initial hot spot in the centre of the bottom wall ($H/D \leqslant 1/2$). Our previous calculations show that for $H/D \geqslant 1$ only a non-axisymmetric flow mode (single roll) is stable, while for $H/D \leqslant 1/2$ even a non-axisymmetric perturbation (like a small inclination in the beginning) leads to axisymmetric flow in the steady state.

If $Ra < Ra_{crit}$, convection is damped out, if $Ra > Ra_{crit}$, the maximum velocity increases again, after the initial perturbation has faded, and reaches a steady-state value in a certain amount of time (Fig. 5). Only in the case of $Ra = Ra_{crit}$, is a steady state reached at which the velocities are very small after fading of the perturbation. In Fig. 6 our results are compared with the experimental and theoretical results of other authors.

3.2. *Velocities and heat transfer*

First, an air-filled cylinder of aspect ratio of $H/D = 1$ is assumed. Figure 7 shows the dependence of the maximum velocity (a) and the Nusselt number (b) on the inclination angle for five different Rayleigh numbers. All graphs ascend, starting at $\alpha = 0°$, up to a maximum, and descend, until a stable stratification is reached at $\alpha = 180°$, which means the hot wall is at the top, the cold wall is at the bottom, no motion occurs, and a linear temperature profile prevails in the axial direction due to pure heat conduction ($Nu = 1$). In the Rayleigh number range of $Ra = 4000$–$21\,500$ the inclination, indicating the abso-

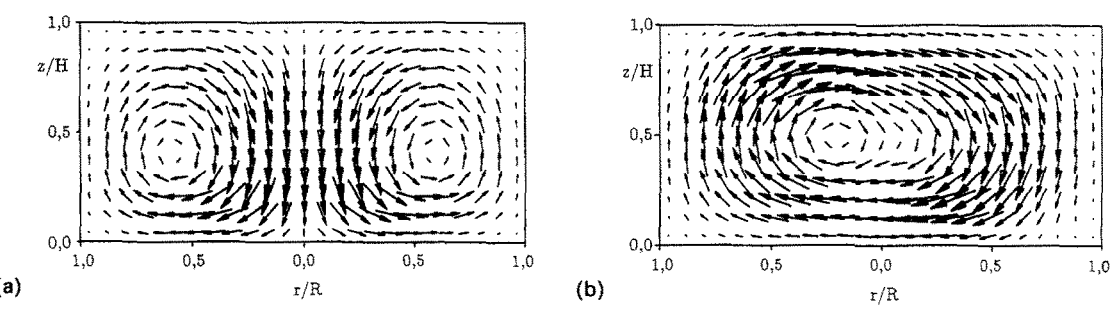

FIG. 4. Flow field in a vertical cross-section ($Ra_D = 40\,000$, $Ra_H = 5000$, $H/D = 1/2$, air): (a) $\alpha = 0°$; (b) $\alpha = 2.5°$.

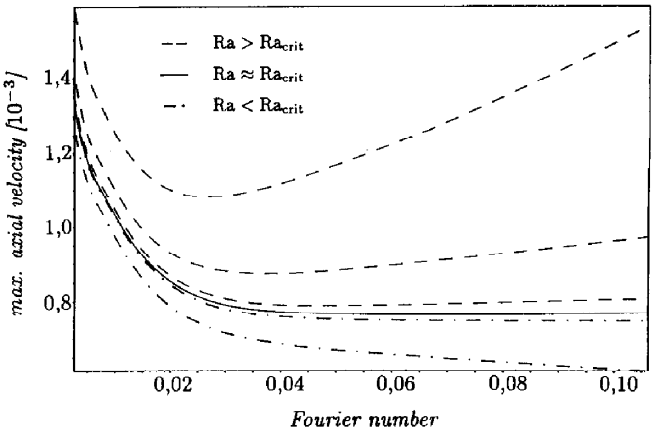

FIG. 5. Determination of the critical Rayleigh number ($H/D = 1$, $\alpha = 0°$, air, perfectly insulated lateral wall).

lute maximum velocity at each Rayleigh number, varies from about 50° to 35°, while the one of the maximum Nusselt number is nearly constant at $\alpha = 50°$–$45°$. At a subcritical Rayleigh number $Ra = 4000$ ($< Ra_{crit} \approx 4300$), no motion is observed at $\alpha = 0°$, however, noticeable convection occurs even at $\alpha = 1°$. This result indicates that in experimental systems, small misalignments of the vertical position of the test chamber may lead to convective flows that should be taken into consideration. At larger Rayleigh numbers, the slope of the graph at $\alpha = 0°$ becomes smaller.

The influence of the fluid properties expressed by the Prandtl number is shown in Fig. 8 for $Ra = 5000$. The general shape of the graphs is independent of the Prandtl number. The data of water are obtained with a finer mesh ((7, 10, 10) instead of (4, 8, 6)), which leads to slightly higher maximum velocities and approximately 5% smaller Nusselt numbers. For fluids with $Pr \gtrsim 0.7$, the Nusselt number is nearly unaffected by the Prandtl number, while there is a certain increase in maximum velocity with increasing Prandtl number. The inclination angles, where the maxima occur, are not influenced by the Prandtl number ($Pr \gtrsim 0.7$). Liquid silicon ($Pr \ll 1$) behaves differently: Nusselt numbers and velocities are significantly smaller. The inclination angles indicating the maxima are shifted to higher values ($\alpha_{max} \approx 65°$–$70°$). Increasing the Rayleigh number to $Ra = 20\,000$ (Fig. 9) affects the shape of the graphs in the manner previously stated; especially at $\alpha = 0°$, velocities increase, and heat transfer is significantly enhanced; but the differences between the fluids are comparable to those at $Ra = 5000$.

Another parameter influencing convection is the aspect ratio. Varying the inclination angle and the aspect ratio simultaneously leads to less comparable results, since the height H is the adequate length scale for $\alpha = 0°$, and the diameter D for $\alpha = 90°$. Here it is assumed that the smaller of the two Rayleigh numbers

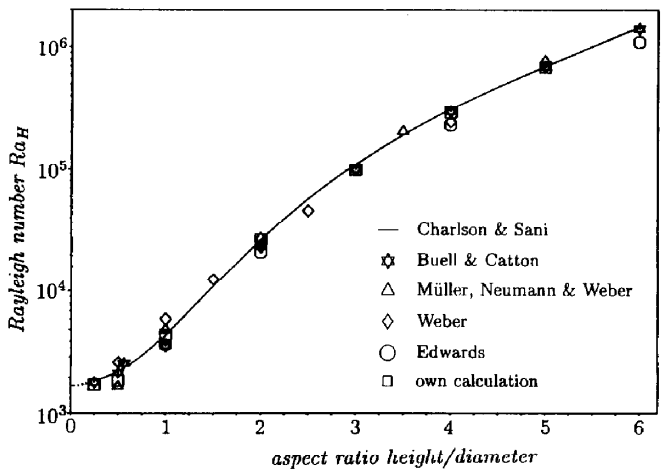

FIG. 6. Calculated critical Rayleigh numbers for vertical cylinders of different aspect ratios in comparison with other authors ($\alpha = 0°$, perfectly insulated lateral wall). Charlson and Sani [32] (theor.), Buell and Catton [33] (theor.), Müller *et al.* [34] (exp., water), Weber [35] (exp., gallium, $Pr = 0.02$), Edwards [36] (theor.).

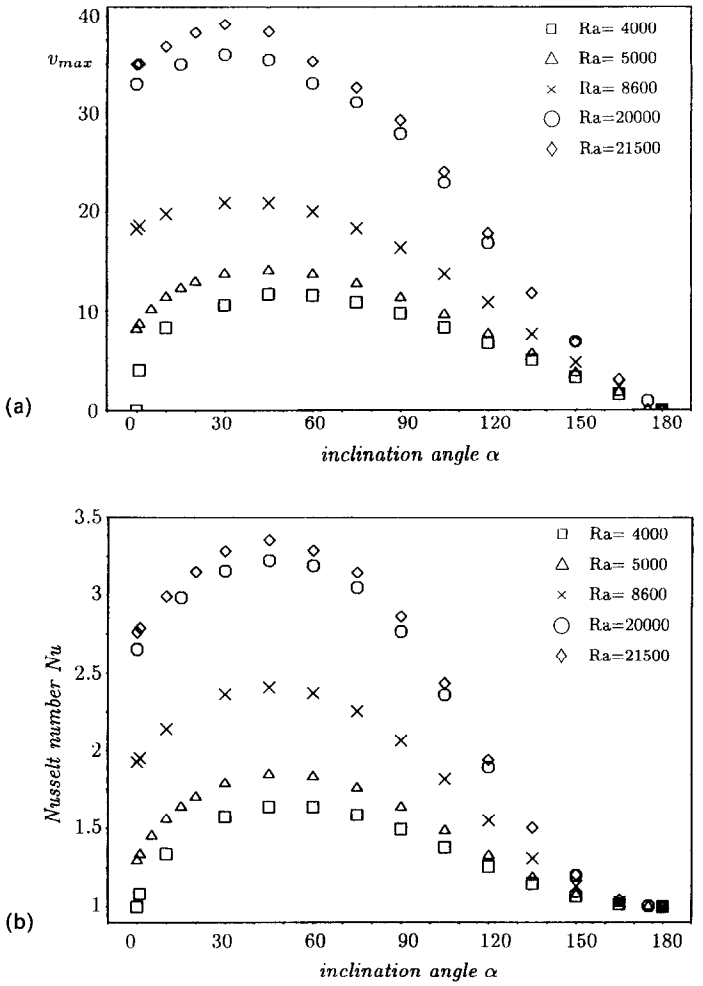

FIG. 7. Maximum dimensionless velocities (a) and Nusselt numbers (b) vs inclination angle α for various Rayleigh numbers (air, $Pr = 0.71$, $H/D = 1$, perfectly insulated lateral wall).

with either D or H as characteristic length is equal to 5000. So the absolute values of the graphs plotted in Fig. 10 are less interesting than their shapes. Increasing the aspect ratio shifts the inclination angles indicating the maxima of velocities and Nusselt numbers to smaller values. For $H/D = 2$, a single roll has always been observed. For $H/D = 1/2$, a change in flow mode causes increasing velocities and heat transfer towards small inclination angles $\alpha \to 0°$. For $\alpha = 0°$ axisymmetric toroidal flow occurs, which is superimposed by a single roll for $\alpha \neq 0°$. Superpositioned flow modes in the vertical cross-section are found for inclination angles up to $\alpha = 3°$. For $\alpha \geqslant 4°$, only the single roll mode is observed. In the cross-section perpendicular to the plane of the main flow, the toroidal structure is found for all inclination angles. The flow at $\alpha = 0°$ is started by a small inclination of $\alpha = 0.01°$ at the first time step. This small non-axisymmetric perturbation leads to an axisymmetric steady-state flow mode. In the literature [34, 37], an additional flow mode of two parallel rolls is predicted. In our calculations, this flow mode is initiated by a slightly higher temperature on a line through the centre of the bottom end wall at the first time step, and it is also found to be stable. But it is considered less probable than the single toroidal roll mode, as it does not develop in the case of the small inclination perturbation.

4. EXPERIMENTAL STUDY

4.1. *Apparatus and instrumentation*

The experimental system is used for determining the dimensionless heat transfer coefficient (Nusselt number). Measurements of the velocity distribution in a cylinder by optical means are very difficult due to refraction effects, as the cylinder's lateral wall behaves like a lense. Even complicated experimental set-ups do not guarantee satisfactory results. Seiler [38] used compensation lenses outside the cylinder wall with the same refraction index as the fluid and the lateral wall to solve this problem. By these means, optical methods become applicable for velocity measurements, but the thermal boundary condition on the lateral wall of the test chamber becomes non-axisymmetric causing flow modes different from those occurring without.

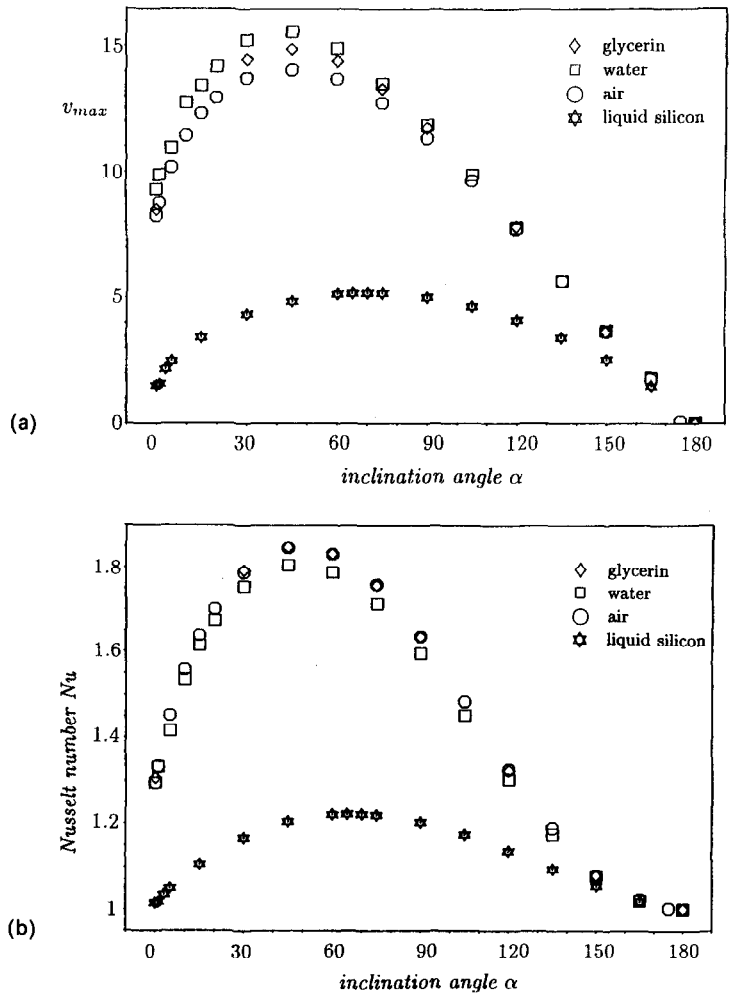

FIG. 8. Maximum dimensionless velocities (a) and Nusselt numbers (b) vs inclination angle for different fluids at $Ra = 5000$ ($H/D = 1$, perfectly insulated lateral wall). Liquid silicon ($Pr = 0.023$), air ($Pr = 0.71$), water ($Pr = 7.1$) and glycerin ($Pr = 135$).

In the experiments reported here, the test fluid helium ($Pr = 0.68$) was contained in a cylindrical enclosure as indicated in Fig. 11. The cylinder was a Plexiglas tube of an inner diameter of 65 mm and a wall thickness of 5 mm. The dimensionless wall admittance for this configuration according to Catton [39] is calculated as

$$C = \frac{k_{\text{fluid}} H}{k_{\text{Plexiglas}} s} = 10.6$$

where s is the wall thickness. This indicates that the lateral wall can be regarded as almost perfectly insulated. The temperature of the cold top end wall, made of a 21 mm thick copper disk, is controlled by a water cooling system. The hot end wall consists of a 6 mm thick copper disk that is electrically heated by a thermofoil heater. To reduce heat losses, it is placed in a copper tub thermally insulated by a 6 mm thick layer of Teflon. The copper tub is heated by a second thermofoil heater (guard heater), and is held at the same temperature as the main heater. In addition, the entire apparatus is thermally insulated towards the ambient by styrofoam plates not shown in Fig. 11. The cylinder is designed for pressures up to 6 bar. Thus, the Rayleigh number can be varied by either changing the gas pressure or the temperature difference between the end walls. The cylinder can be inclined perpendicular to its axis from 0° to 180°. An aspect ratio of $H/D = 1$ is chosen in the experiments reported here.

To measure the temperatures, three thermocouples (NiCr–Ni) are installed in the cold top end wall, 12 in the lateral wall, four in the warm bottom end wall, and two in the tub of the guard heater. The pressure is measured electrically by a pressure transducer. A digital computer is used to control the experiment, and for data storage. Thermocouples are scanned every 30 s, then the temperatures are calculated. The power supplies of the heaters are controlled by a digital PID-controller and a digital–analogue converter. If the temperature differences between the cold and the warm walls and the guard heater tub, respectively, deviate less than a certain amount from the nominal value for 50 succeeding time steps, steady-state con-

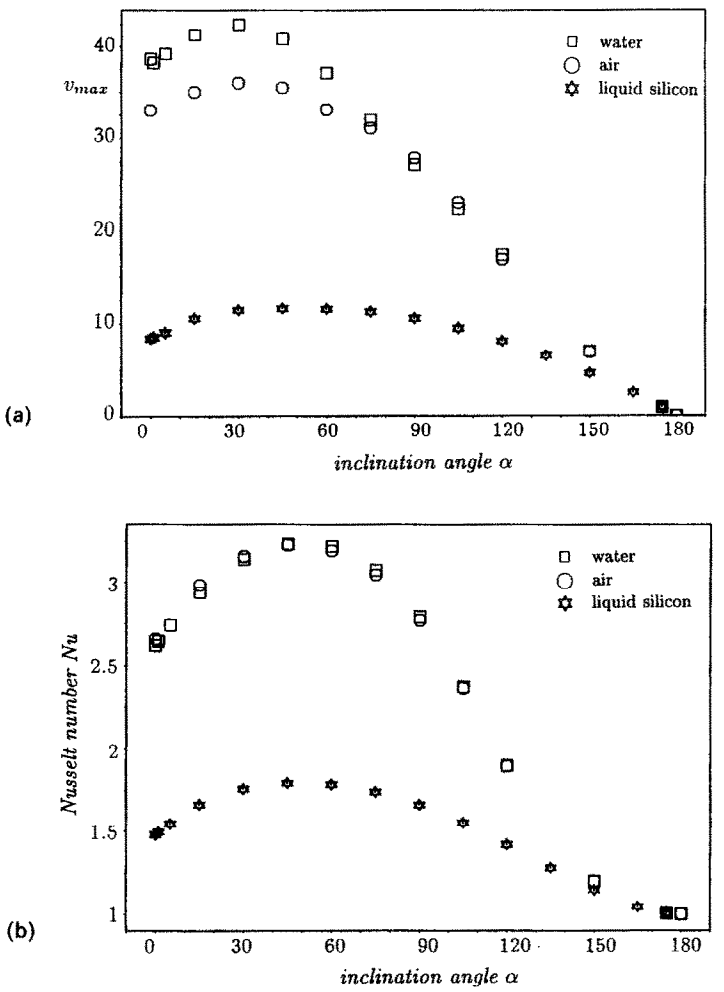

FIG. 9. Maximum dimensionless velocities (a) and Nusselt numbers (b) vs inclination angle for different fluids at a larger Rayleigh number of $Ra = 20\,000$ ($H/D = 1$, perfectly insulated lateral wall).

ditions are assumed to prevail. Then the heating power of the main heater is measured and recorded for about 100–200 time steps, until the last three actual values are equal to the mean value or do not change the mean value significantly. When measuring the heating power at $\alpha = 180°$ (stable density stratification), pure conduction occurs. So the heat loss can be determined as the difference between the measured heating power and the calculated conductive heat flux in the fluid. The heat loss is determined at every pressure level and temperature difference used, and for various ambient temperatures. So the influence of the ambient temperature is taken into account. It is assumed that the heat losses are independent of the inclination angle. Thus the Nusselt number is calculated as

$$Nu(\alpha) = \frac{\text{heating power}(\alpha, T_\infty) - \text{heat loss}(T_\infty)}{\text{conductive heat flux}}.$$

4.2. *Experimental results*

As already mentioned, the Plexiglas lateral wall is supposed to be insulating rather than conducting. This assumption is verified by comparison with calculated results for either a perfectly insulated or a perfectly conducting wall. The test fluid helium ($Pr = 0.68$), which is comparable to air ($Pr = 0.71$), is used in the calculations presented in Fig. 12. The numerical results which show the dependence of the Nusselt number on the inclination angle are confirmed by the experimental data. These are closer to the calculated Nusselt number for a perfectly insulated lateral wall than to those for a perfectly conducting one.

Figure 13 shows the effect of inclination on the Nusselt number for various Rayleigh numbers. At all Rayleigh numbers, maximum heat transfer is observed at inclination angles of $\alpha \approx 45°$–$60°$. (The inclination is varied in increments of 15°. Therefore, the inclination angle corresponding to maximum heat flux is not determined more exactly.) No increase in the Nusselt number at $\alpha \to 0°$ is observed, which is in agreement with the numerical result that no toroidal flow will occur at an aspect ratio of $H/D = 1$.

The result that maximum heat transfer in a cylinder of $H/D = 1$ occurs at inclination angles of $\alpha \approx 45°$–

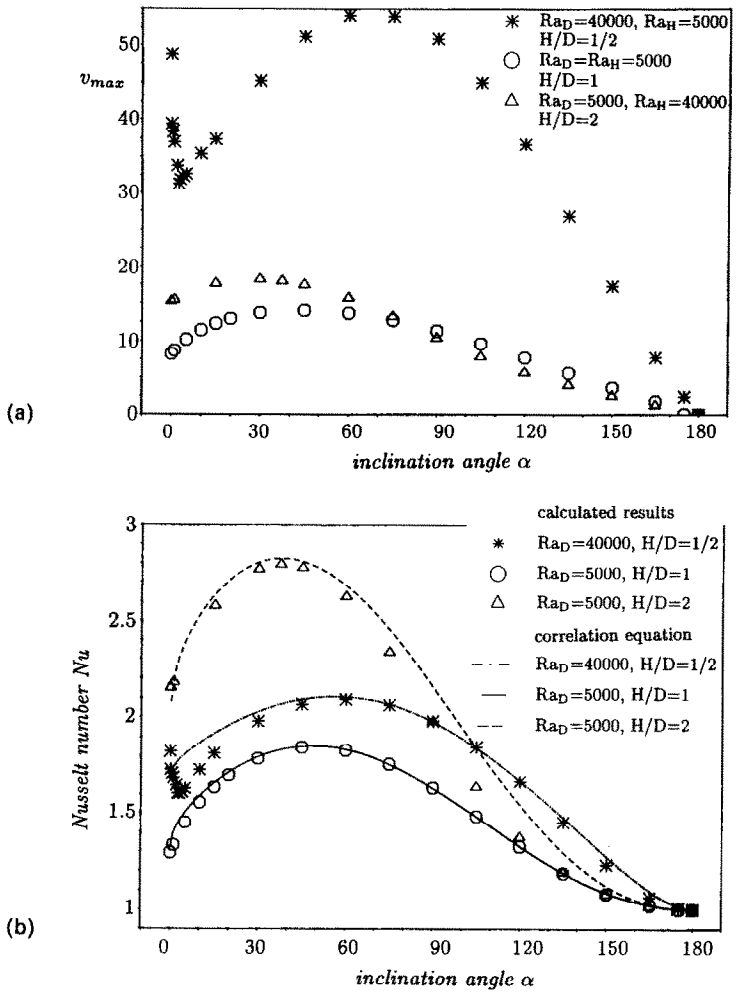

FIG. 10. Maximum dimensionless velocities (a) and Nusselt numbers (b) vs inclination angle for different aspect ratios (air, perfectly insulated lateral wall); (b) also contains graphs obtained with correlation (8).

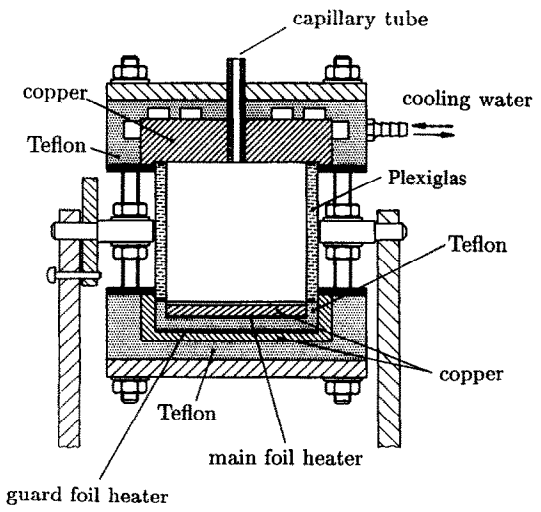

FIG. 11. Schematic cross-section of the experimental apparatus.

60°, differs from findings for cavities of $H/D \to 0$, where the heat flux maxima are observed at $\alpha = 0°$ or 90°. However, they are in general agreement with results for convection in rectangular boxes or channels with moderate aspect ratios [14, 15, 19].

The variation of heat flux with the Rayleigh number is presented in Fig. 14 for an inclination angle of $\alpha = 90°$. The calculations and measurements lead to comparable results, although the graph of the calculated values is steeper due to the assumption of a perfectly insulated lateral wall.

5. CORRELATION FOR THE NUSSELT NUMBER

The results for a perfectly insulated lateral wall for a cylindrical enclosure presented here and the findings in ref. [25] can be correlated by the following equation:

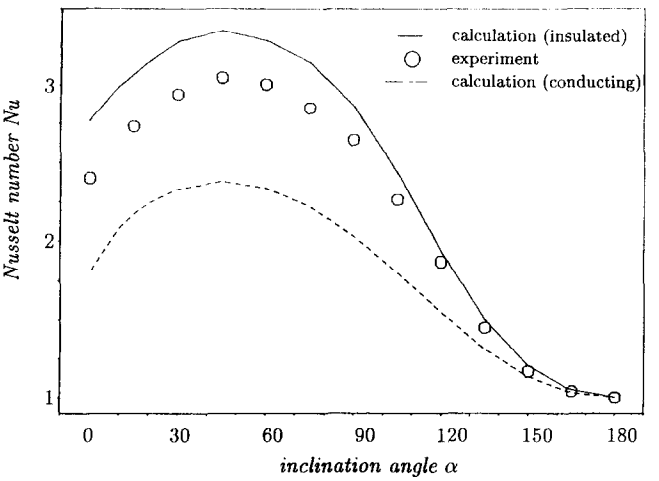

FIG. 12. Comparison of measured Nusselt numbers with calculated values for either a perfectly conducting or perfectly insulated lateral wall ($Ra = 21\,500$, $H/D = 1$, air or helium, respectively).

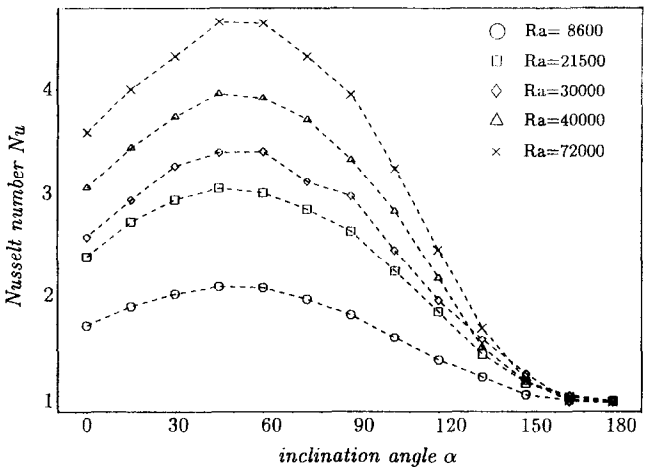

FIG. 13. Measured Nusselt number vs inclination angle α for various Rayleigh numbers ($H/D = 1$, helium).

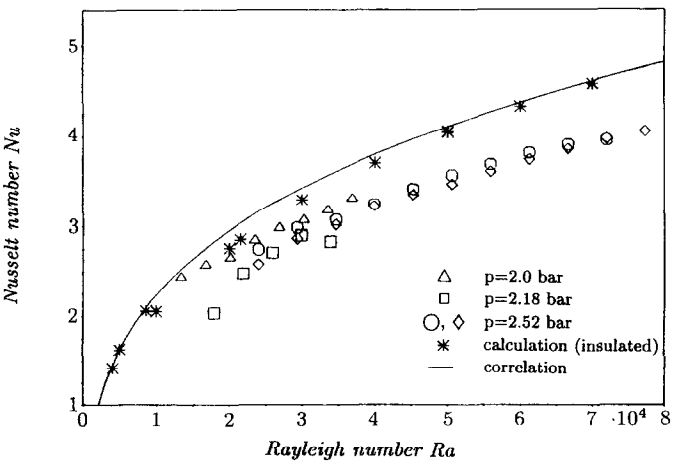

FIG. 14. Nusselt number vs Rayleigh number. Comparison of calculated and measured results with data obtained from equation (8) ($H/D = 1$, $\alpha = 90°$).

$$Nu = 1+0.052\left(\frac{\frac{H}{D}-0.1}{0.9}\right)^{-1/2}\left[(\sin\alpha)^{1/2}+1.3\left(\frac{H}{D}\right)^{3/4}(1+\cos\alpha)^{1/2}\right]^3+0.42[(Ra_D)^{1/4}-(5000)^{1/4}][2(\cos(\alpha/2))^{1/2}-\cos(\alpha/2)]^4. \quad (8)$$

Equation (8) is valid for $4000 \leqslant Ra_D \leqslant 80\,000$, $0° \leqslant \alpha \leqslant 180°$, $1/2 \leqslant H/D \leqslant 2$ and $Pr \gtrsim 0.7$. Since the Nusselt number does not seem to change dramatically, when the Prandtl number is enhanced, the equation can also be used for fluids with $Pr \gtrsim 0.7$. Due to the lack of data, the Prandtl number influence for $Pr < 0.7$ is not considered in correlation (8), as it cannot be described quantitatively over a large range with confidence, and is therefore left out. As a proof, data evaluated with the help of equation (8) are compared with numerical and experimental results in Figs. 10(b) and 14.

6. CONCLUSION

A numerical code for calculating three-dimensional laminar natural convection in a fluid-filled cylindrical enclosure heated at one end wall and cooled at the other one has been developed and verified by experiments. The code is extensively tested, and is found to produce results that are in agreement with data from the literature and present experiments.

In the case of a cylinder with an aspect ratio of $H/D \geqslant 1$, three-dimensional non-axisymmetric flow modes are found. This flow can by no means be approximated by two-dimensional calculations, as it is possible for horizontal fluid layers of small aspect ratios of $H/D \to 0$. Maximum heat transfer is found at inclination angles of $\alpha \approx 45°$–$60°$ for $H/D = 1$. With an increasing aspect ratio, the maximum shifts to smaller inclination angles. The Prandtl number has a minor influence for $Pr \gtrsim 0.7$, while heat transfer and flow velocities decrease with decreasing Prandtl number in the range of $Pr < 0.7$. As a result, for technical applications where heat transfer is to be enhanced, it is recommended to incline a cavity by about 45°.

The computer code is able to calculate transient processes as well. In connection with materials processing under microgravity, the question arises, whether convection has to be taken into account or not. The quasi-steady gravity is of the order of 10^{-5} the gravity level on earth, but the transient accelerations are up to 1000 times larger than that. Thus, the code is used to calculate convection developing from a state of weightlessness and rest, when gravity pulses of definite shape, amplitude, and frequency or duration are applied [25–27, 31].

Acknowledgement—The work reported here is part of a doctoral thesis in mechanical engineering of the first author. It was financially supported by grants from the Bavarian government and from 'Loschge-Studienstiftung' which is gratefully acknowledged.

REFERENCES

1. E. L. Koschmieder, Bénard convection, *Adv. Chem. Phys.* **26,** 177–211 (1974).
2. G. H. Schiroky and F. Rosenberger, Free convection of gases in a horizontal cylinder with differentially heated end walls, *Int. J. Heat Mass Transfer* **27,** 584–598 (1984).
3. C. Smutek, P. Bontoux, B. Roux, G. H. Schiroky, A. C. Hurford, F. Rosenberger and G. deVahl Davis, Three-dimensional convection in horizontal cylinders: numerical solutions and comparison with experimental and analytical results, *Numer. Heat Transfer* **8,** 613–631 (1985).
4. P. Bontoux, B. Roux, G. H. Schiroky, B. L. Markham and F. Rosenberger, Convection in the vertical midplane of a horizontal cylinder. Comparison of two-dimensional approximations with three-dimensional results, *Int. J. Heat Mass Transfer* **29,** 227–240 (1986).
5. P. Bontoux, C. Smutek, B. Roux and J. M. Lacroix, Three-dimensional buoyancy-driven flows in cylindrical cavities with differentially heated endwalls—1. Horizontal cylinders, *J. Fluid Mech.* **169,** 211–227 (1986).
6. A. Bejan and C. L. Tien, Laminar natural convection heat transfer in a horizontal cavity with different end temperatures, *J. Heat Transfer* **100,** 641–647 (1978).
7. A. Bejan and C. L. Tien, Fully developed natural counterflow in a long horizontal pipe with different end temperatures, *Int. J. Heat Mass Transfer* **21,** 701–708 (1978).
8. S. Kimura and A. Bejan, Experimental study of natural convection in a horizontal cylinder with different end temperatures, *Int. J. Heat Mass Transfer* **23,** 1117–1176 (1980).
9. S. Kimura and A. Bejan, Numerical study of natural circulation in a horizontal duct with different end-temperatures, *Wärme- und Stoffübertr.* **14,** 269–280 (1980).
10. P. Bontoux, C. Smutek, A. Randriamampianina, B. Roux, G. P. Extrémet, A. C. Hurford, F. Rosenberger and G. deVahl Davis, Numerical solutions and experimental results for three dimensional buoyancy driven flows in tilted cylinders, *Adv. Space Res.* **6**(5), 155–160 (1986).
11. D. Dropkin and E. Somerscales, Heat transfer by natural convection in liquids confined by two parallel plates which are inclined at various angles with respect to the horizontal, *J. Heat Transfer* **87,** 77–84 (1965).
12. I. Catton, P. S. Ayyaswamy and R. M. Clever, Natural convection flow in a finite, rectangular slot arbitrarily oriented with respect to the gravity vector, *Int. J. Heat Mass Transfer* **17,** 173–184 (1974).
13. J. N. Arnold, I. Catton and D. K. Edwards, Experimental investigation of natural convection in inclined rectangular regions of differing aspect ratios, *J. Heat Transfer* **98,** 67–71 (1976).
14. H. Ozoe, K. Yamamoto, H. Sayama and S. W. Churchill, Natural circulation in an inclined rectangular channel heated on one side and cooled on the opposing side, *Int. J. Heat Mass Transfer* **17,** 1209–1217 (1974).
15. H. Ozoe, H. Sayama and S. W. Churchill, Natural convection in an inclined square channel, *Int. J. Heat Mass Transfer* **17,** 401–406 (1974).
16. H. Ozoe, H. Sayama and S. W. Churchill, Natural convection in an inclined rectangular channel at various aspect ratios and angles—experimental measurements, *Int. J. Heat Mass Transfer* **18,** 1425–1431 (1975).
17. H. Ozoe, H. Sayama and S. W. Churchill, Natural convection patterns in a long inclined rectangular box heated from below—1. Three-dimensional photography, *Int. J. Heat Mass Transfer* **20,** 123–129 (1977).
18. H. Ozoe, K. Yamamoto, H. Sayama and S. W. Churchill,

Natural convection patterns in a long inclined rectangular box heated from below—2. Three-dimensional numerical results, *Int. J. Heat Mass Transfer* **20,** 131–139 (1977).
19. W. M. M. Schinkel, Natural convection in inclined air-filled enclosures, Dutch Efficiency Bureau, Pijnacker (1980).
20. K. R. Kirchartz, Zeitabhängige Zellularkonvektion in horizontalen und geneigten Behältern, Doctoral Thesis, Univ. (TH) Karlsruhe (1980).
21. K. R. Kirchartz, H. Oertel, Jr. and J. Zierep, Time-dependent convection. In *Convective Transport and Instability Phenomena* (Edited by J. Zierep and H. Oertel, Jr.), pp. 101–122. Verlag G. Braun, Karlsruhe (1982).
22. K. R. Kirchartz, Numerische Simulation von Strukturänderungen bei dreidimensionalen Konvektionsströmungen, *Z. Flugwiss. Weltraumforschung* **13,** 1–7 (1989).
23. S. J. M. Linthorst, W. M. M. Schinkel and C. J. Hoogendoorn, Flow structure with natural convection in inclined air-filled enclosures, *Natural Convection in Enclosures, Proc. 19th Natn. Heat Transfer Conf.*, Orlando, Florida, ASME-HTD Vol. 8, pp. 39–45 (1980).
24. R. A. Wirtz and W. F. Tseng, Natural convection across tilted, rectangular enclosures of small aspect ratio, *Natural Convection in Enclosures, Proc. 19th Natn. Heat Transfer Conf.*, Orlando, Florida, ASME-HTD Vol. 8, pp. 47–54 (1980).
25. S. Schneider, Laminare, freie Konvektion in einem Zylinder bei konstanter und zeitveränderlicher Schwerkraft (g-jitter), Doctoral Thesis, Technische Universität München (1990).
26. A. Heiss, S. Schneider and J. Straub, g-jitter effects on natural convection in a cylinder: a three-dimensional numerical calculation, *Proc. 6th Europ. Symp. on Material Sciences under Microgravity Conditions*, Bordeaux (ESA SP-256), pp. 517–523 (1986).
27. S. Schneider and J. Straub, Natural convection in a cylinder caused by gravitational interferences: a three-dimensional numerical calculation. In *Int. Symp. on Thermal Problems in Space-based Systems* (Edited by F. Dobran and M. Imber), ASME-HTD Vol. 83, pp. 77 83. New York (1987).
28. S. V. Patankar, *Numerical Heat Transfer and Fluid Flow*. Hemisphere/McGraw-Hill, New York (1980).
29. F. H. Harlow and J. E. Welch, Numerical calculation of time-dependent viscous incompressible flow of fluid with free surface, *Physics Fluids* **8,** 2182–2189 (1965).
30. G. deVahl Davis, A note on a mesh for use with polar coordinates, *Numer. Heat Transfer* **2,** 261–266 (1979).
31. S. Schneider and J. Straub, Influence of the Prandtl number on laminar natural convection in a cylinder caused by g-jitter, *J. Cryst. Growth* **97,** 235–242 (1989).
32. G. S. Charlson and R. L. Sani, On thermoconvective instability in a bounded cylindrical fluid layer, *Int. J. Heat Mass Transfer* **14,** 2157–2160 (1971).
33. J. C. Buell and I. Catton, The effect of wall conduction on the stability of a fluid in a right circular cylinder heated from below, *J. Heat Transfer* **105,** 255–260 (1983).
34. G. Müller, G. Neumann and W. Weber, Natural convection in vertical Bridgman configurations, *J. Cryst. Growth* **70,** 78–93 (1984).
35. W. Weber, Untersuchung der thermischen Auftriebskonvektion in Modellsystemen zur Kristallzüchtung bei normaler und erhöhter Schwerkraft, Doctoral Thesis, Univ. Erlangen-Nürnberg (1988).
36. D. K. Edwards, Subsequent discussion of W. L. Heitz and J. W. Westwater, Critical Rayleigh numbers for natural convection of water confined in square cells with L/D from 0.5 to 8, *J. Heat Transfer* **93,** 188–196 (1971).
37. G. Neumann, Three-dimensional numerical simulation of buoyancy-driven convection in vertical cylinders heated from below, *J. Fluid Mech.* **214,** 559–578 (1990).
38. G. A. Seiler, Experimentelle Untersuchung der überkritischen Konvektionsströmung in einem Zylinder des Verhältnisses Höhe/Durchmesser = 1, Doctoral Thesis, Univ. (TH) Karlsruhe (1988).
39. I. Catton, Effect of wall conduction on the stability of a fluid in a rectangular region heated from below, *J. Heat Transfer* **94,** 446–452 (1972).

CONVECTION LAMINAIRE NATURELLE DANS UNE ENCEINTE CYLINDRIQUE AVEC DES TEMPERATURES DIFFERENTES AUX EXTREMITES

Résumé—La convection laminaire naturelle dans un cylindre empli de fluide, avec des températures différentes aux extrémités, est étudiée numériquement en tridimensionnel et vérifiée expérimentalement. On présente les influences des paramètres du fluide et de la géométrie, comme le nombre de Rayleigh ($Ra < 8 \times 10^4$), le nombre de Prandtl ($0{,}023 \leqslant Pr \leqslant 135$), le rapport de forme hauteur/diamètre ($0{,}5 \leqslant H/D \leqslant 2$) et l'angle d'inclinaison ($0° \leqslant \alpha \leqslant 180°$) sur le mouvement convectif et le transfert de chaleur. Le maximum de transfert et les plus grandes vitesses sont trouvés pour $H/D = 1$ à des angles d'inclinaison $\alpha \simeq 45°$–$60°$.

LAMINARE FREIE KONVEKTION IN EINEM ZYLINDER DES HÖHEN-DURCHMESSER-VERHÄLTNISSES 1 MIT UNTERSCHIEDLICH TEMPERIERTEN STIRNFLÄCHEN

Zusammenfassung—Die freie Konvektion in einem fluidgefüllten Zylinder, dessen Stirnflächen unterschiedlich temperiert sind, wird in einer dreidimensionalen numerischen Analyse untersucht und experimentell überprüft. Die Einflüsse der Rayleighzahl ($Ra < 8 \times 10^4$), der Prandtlzahl ($0.023 \leqslant Pr \leqslant 135$), des Längenverhältnisses Höhe/Durchmesser ($1/2 \leqslant H/D \leqslant 2$) und des Neigungswinkels ($0° \leqslant \alpha \leqslant 180°$) werden aufgezeigt. Der größte Wärmeübergang und die größten Strömungsgeschwindigkeiten treten bei $H/D = 1$ im Winkelbereich $\alpha \approx 45°$–$60°$ auf.

ЛАМИНАРНАЯ ЕСТЕСТВЕННАЯ КОНВЕКЦИЯ В ЦИЛИНДРИЧЕСКОЙ ЗАМКНУТОЙ ПОЛОСТИ С РАЗЛИЧНЫМИ КОНЦЕВЫМИ ТЕМПЕРАТУРАМИ

Аннотация—Ламинарная естественная конвекция в заполненном жидкостью цилиндре с различными температурами стенки на концах исследуется численно с помощью трехмерного метода и подтверждается экспериментально. Показано влияние таких параметров жидкости и геометрии цилиндра, как числа Рэлея ($Ra < 8 \times 10^4$): Прандтля ($0{,}023 \leqslant Pr \leqslant 135$). отношеуия высоты к диаметру ($0{,}5 \leqslant H/D \leqslant 2$) и угла наклона ($0° \leqslant \alpha \leqslant 180°$) на конвективное движение и теплообмен. Получены максимальные значения интеисивности теплообмена и скорости для $H/D = 1$ при $\alpha \approx 45°–60°$.